RESEARCH PAPER

Fragility Assessment for Horizontally Curved Reinforced Concrete Box Girder Bridges Using As-built Data

Arya Zamiri[1] · Mohammad-Reza Banan[1] · Mahmoud-Reza Banan[1]

Abstract

Damage to one or multiple components of a bridge could result in various conditions, extended from a cosmetically repairable damage to jeopardizing life safety of the users. Fragility curves are beneficial in seismic risk assessment. Due to the limitations of the transformation network, aesthetic considerations, etc., a bridge might be skewed or curved which makes the problem more complex. Fragility assessment of bridges utilizing dynamic analysis seems to be inevitable in reducing damage levels in future earthquakes. In this study, the effectiveness of adopting fragility curves in performance evaluation and risk assessment of bridges is investigated. It is done by considering a highway curved bridge with eleven piers. FEM model is developed using OpenSees platform. Time history dynamic analysis is used to obtain the displacements and forces as demands of each bridge component. Eventually, fragility curves are developed for four damage states. Pier fragility curves of this bridge depict a very appropriate behavior under various levels of excitation which could be related to the appropriate distance of the stirrups. Prevalent mode of the bridge causes torsion in the first bay of the bridge. In the other two bays, only longitudinal transfer of the deck was observed. Bearing fragility curves of the bridge depict fair results in the transverse direction due to the presence of the shear keys as opposed to the longitudinal direction.

1 Introduction

Recent earthquakes have proven the bridges as the weakest links and more susceptible to damage in the transportation network. Severe damages to these links could result in catastrophic consequences in the aftermath of a seismic incident. In the last few decades, various studies have been done on fragility computation of the bridges, making the subject a rather novel one Ramanathan et al. (2010), Kaviani et al. (2012) and Padgett et al. (2008). However, the number of studies on horizontally curved box girder bridges is limited. There are some studies pertaining to combined effect of responses in curved bridges (Tondini and Stojadinović 2012; Monzon et al. 2013).

One of the major tools at our disposal in the field of risk assessment of the structures is fragility curves. These curves represent the probability of exceeding a specific damage scenario under a specified seismic excitation for a given structure. Some characteristics of a bridge such as material characteristics, damping ratio, mass, accelerations and velocity of applied loads are influential in bridge response assessment under dynamic loadings. In general, it is presumed that considering probabilistic approaches as opposed to deterministic ones is more desirable because they give a balance between safety and cost. By producing fragility curves for various bridge components in the as-built condition of the existing structures, the weak components of the bridge structural system are identified.

In the field of transportation and highway design, using bridges with complex geometries and structural systems, i.e., singly curved or doubly curved, whether reinforced concrete or steel bridges, is inevitable. Accelerating traffic flow, structural limitations and intermittently augmenting aesthetic design force designers to utilize the curved bridge concept in their work Itani and Reno (2000). There are limited numbers of studies pertaining to fragility analysis of this structural system, i.e., horizontally doubly curved box girder decks with various subtended angles. The complex behavior of horizontally curved bridges during the earthquake incident

✉ Mohammad-Reza Banan
  banan@shirazu.ac.ir

[1] Department of Civil and Environmental Engineering, Shiraz University, Shiraz, Iran

versus that of the straight ones makes the fragility analysis of these systems crucial regarding the seismic risk assessment of the bridges. Seismic loading and service loading have been observed to have different sorts of interactions on bridges (Nutt et al. 2008).

Iran is surrounded by multiple major faults such as Eurasia fault, Arabian Peninsula fault and Indian Ocean fault. Thus, most regions of Iran are at high seismic risk. Fragility curves are developed by considering a wide spectrum of relevant ground accelerations or velocities. Although the structural system of a bridge is designed for a specific design

acceleration, the probability of experiencing a severe earthquake during its service life span still exists. By using the fragility curves, one can safely predict the bridge behavior and performance levels under different earthquake scenarios.

Even numerous construction projects of reinforced concrete bridges with different geometry and structural systems have been accomplished in Iran; however, the seismic analysis and fragility curve development studies for these types of structures are few. Further studies are required for risk assessment of bridges in Iran.
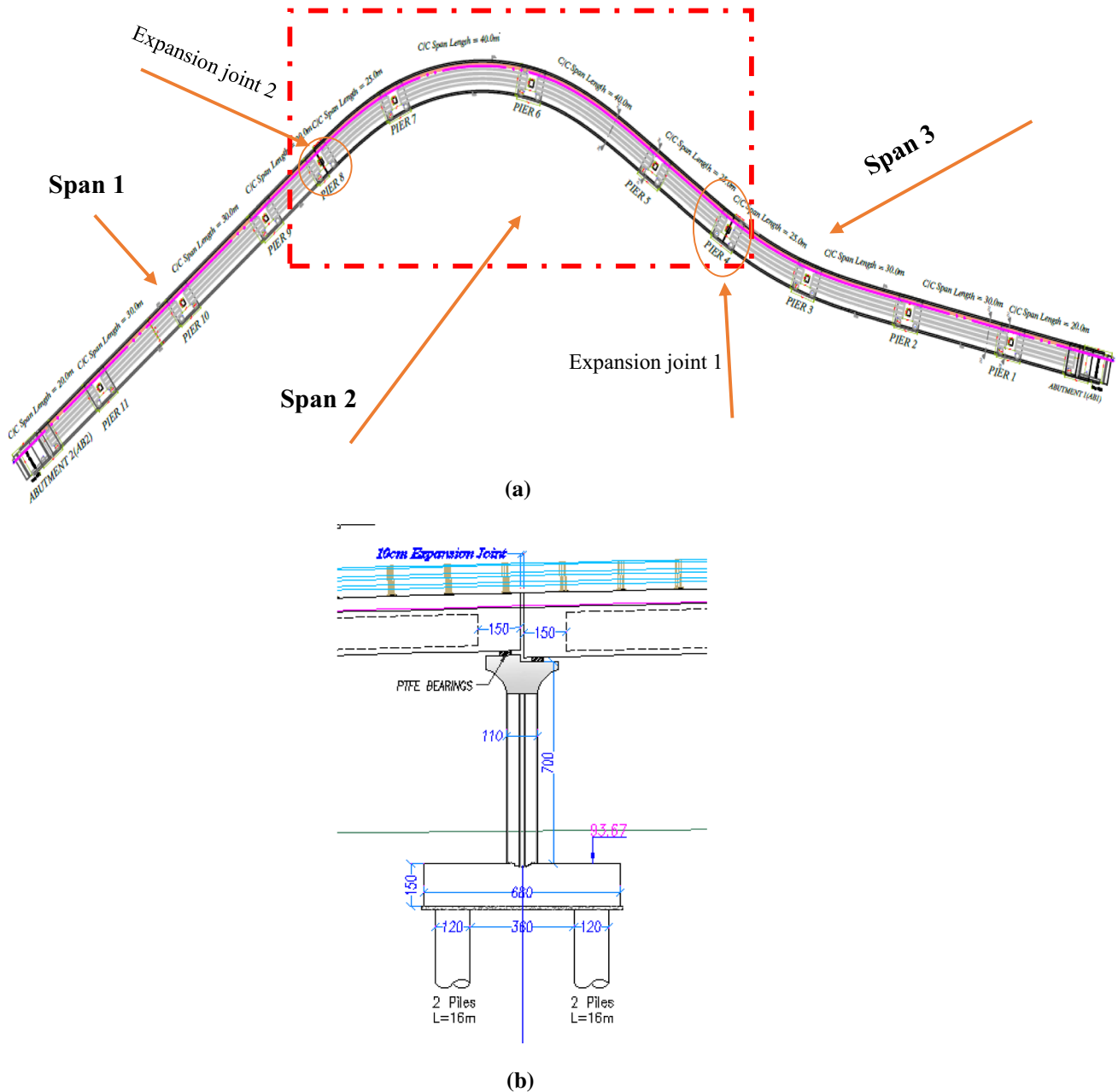

Fig. 1 **a** Typical as-built bridge plan with double curvature box girder deck. 83 degrees subtended angle of span 2 as opposed to 30 degrees subtended angle of span 3. **b** Pier at the expansion joint with PTFE/Elastomeric Bearing
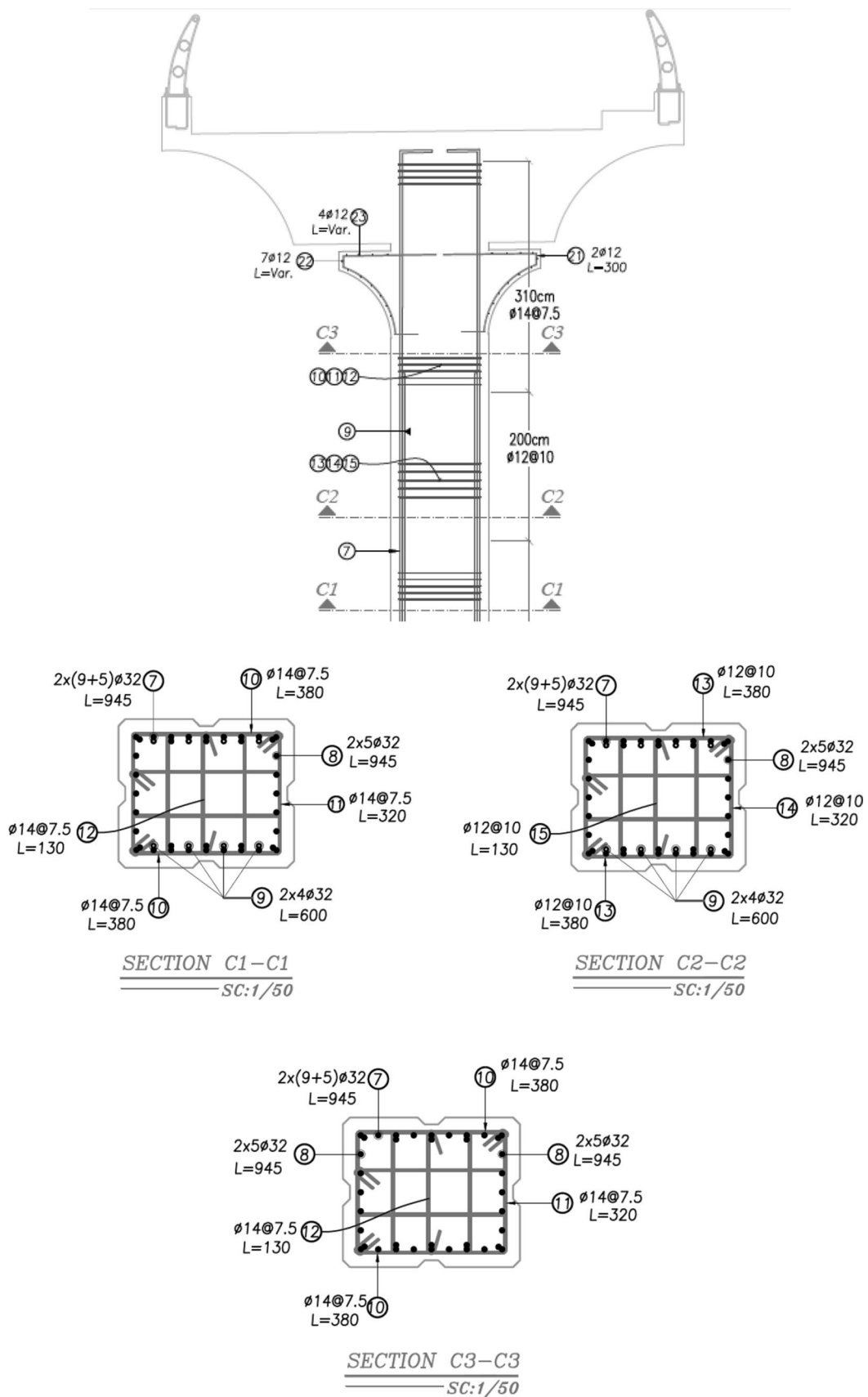
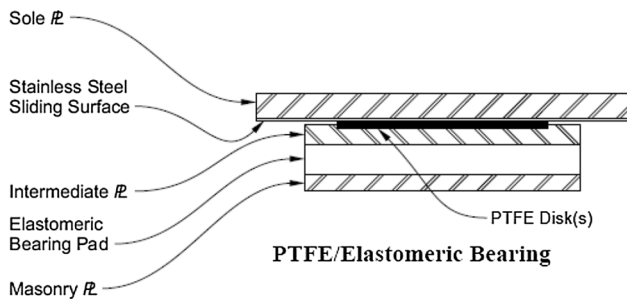**Fig. 2** Reinforcing steel details of a typical pier

Fig. 3 PTFE/elastomeric bearing model and hysteretic behavior (Ramanathan 2012)
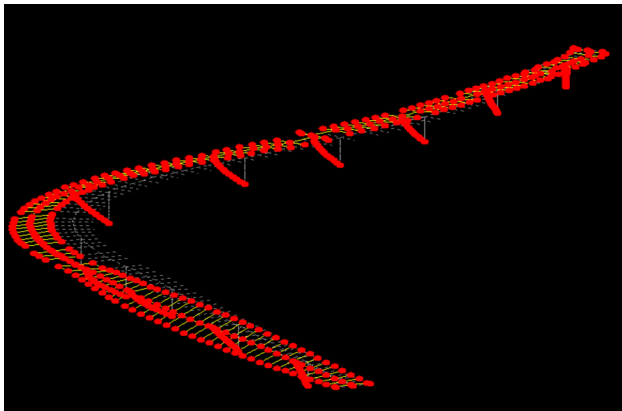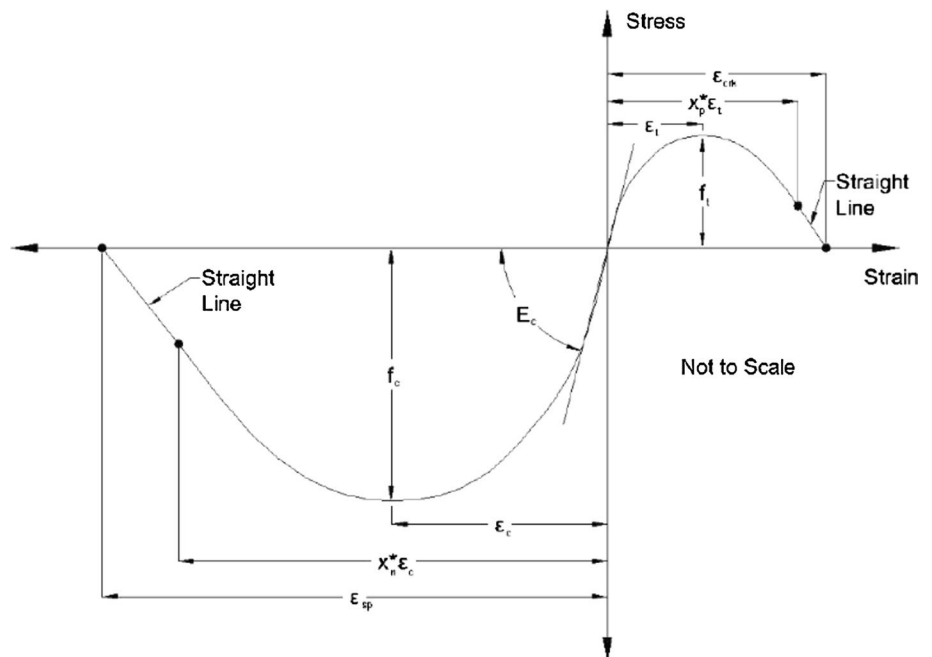

Fig. 4 3D finite element model and the first mode of the bridge obtained using OpenSees platform

This study aims at evaluation of seismic fragility curves for horizontally curved single pier reinforced concrete box

Fig. 5 Concrete07 Mander model

girder bridges.

Detailed 3D finite element models of a specific bridge class are developed and analyzed under various suites of ground motion records using the OpenSees platform Open-Sees (2005). The results obtained from dynamic analyses of these bridge models are studied and post-processed in order to calculate the component and system fragility curves.

2 Fragility Curve Development

Fragility curves represent the probability of damage or destruction of a given structure under different base excitations. If P_f is defined as the probability of damage in the specific level under a specific base excitation, D is defined as the demand imposed on the structure, C_i is defined as the capacity in the level i, then the damage to the structure or its components is defined as $C \leq D$; under these circumstances, the probability of seismic fragility is defined as Eq. (1). With IM_j being the intensity measure which in this study is assumed as the peak ground acceleration (PGA) (Eq. 1a), the engineering demand parameter, EDP, has a logarithmic relation with IM, i.e., PGA as shown in Eq. 1b (Cornell et al. 2002)

$$P_f = P[D \geq C | IM_j] \tag{1a}$$

$$EDP = aIM^b. \tag{1b}$$

Another mathematical approach for analytical fragility curves is presented here in Eq. (2)
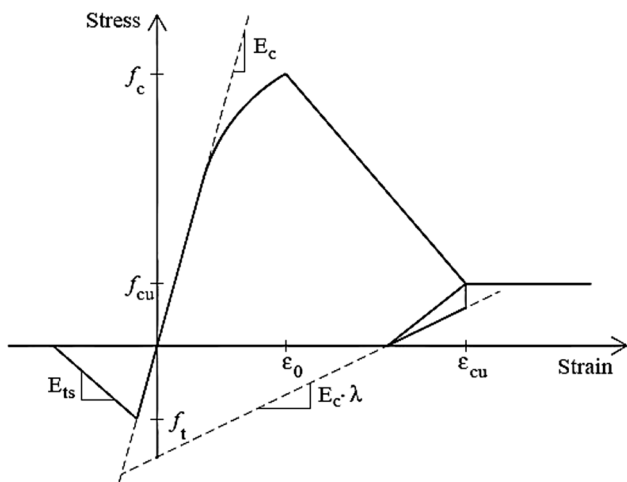
Fig. 6 Stress–strain relations in Concrete01 model

$$P_{\mathrm{f}} = \phi \left\{ \frac{\ln \frac{S_{\mathrm{d}}}{S_{\mathrm{c}}}}{\beta} \right\}. \tag{2}$$

In Eq. (2), S_{d} is the median of the demand on the structure, S_{c} is the median of the capacity of the structure, β is the logarithmic standard deviation of the structure presented by Eq. (3), and Φ is the standard normal cumulative distribution function

$$\beta = \sqrt{\beta_{\mathrm{d}|IM}^2 + \beta_{\mathrm{c}}^2}. \tag{3}$$

In Eq. (3), $\beta_{\mathrm{d}|IM}$ is a representation of the dispersion of the demand conditioned on a given intensity measure and the seismic capacity, C, can be obtained from experimental results and expert opinion with statistical characteristics S_{c} as median of the capacity and β_{c} as standard deviation of capacity. By combining the three equations above, one can obtain the probabilistic seismic demand model representation of the bridge probability of failure for a given performance level as given by Eq. (4)

$$P[D \geq C | \mathrm{IM}_j] = \phi \left(\frac{\ln S_{\mathrm{d}} - \ln S_{\mathrm{c}}}{\sqrt{\beta_{\mathrm{d}|IM}^2 + \beta_{\mathrm{c}}^2}} \right). \tag{4}$$

Seismic demand of the structure is the response of the structure under a specific seismic excitation and is a representation of the degree of excitation and damage to the structure.

Fragility curves can be developed by three different methods: (1) experimental fragility curves, (2) analytical fragility curves and (3) hybrid fragility curves which are a combination of the last two methods. Due to lack or limited number of records of previous earthquakes and bridge responses for a specific seismic zone and bridge site, the method utilized for this study is analytical fragility curve method. To develop analytical fragility curves, different dynamic analysis methods such as nonlinear static analysis, response history spectrum analysis, nonlinear time history analysis, incremental dynamic analysis (IDA) (FEMA-350 2000), the nonlinear time history analysis can be used.

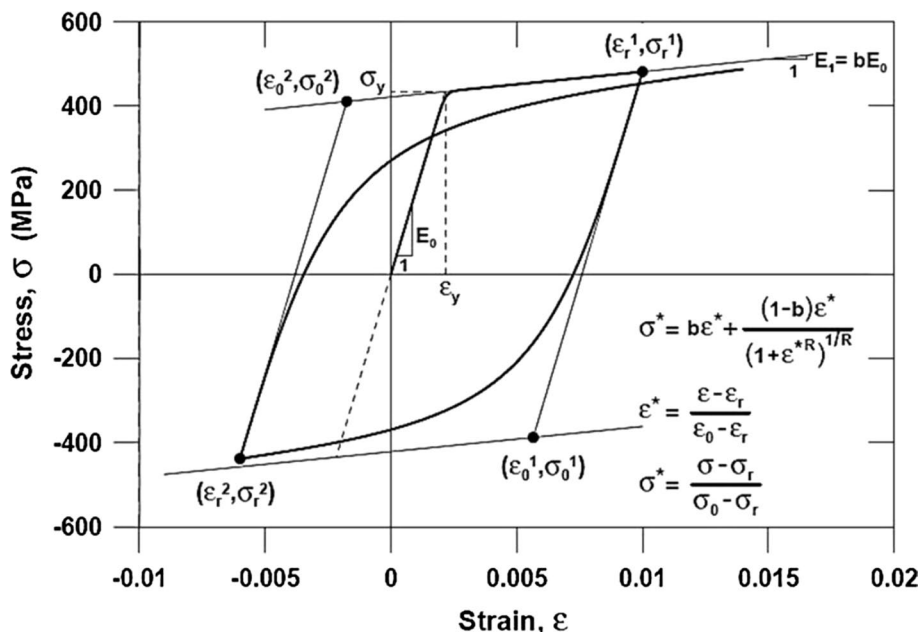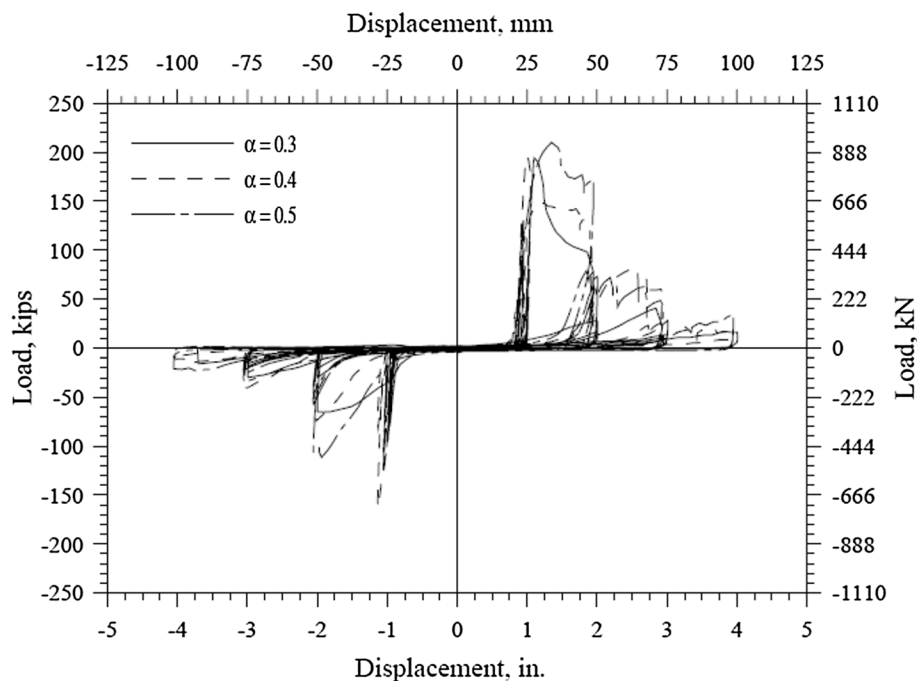**Fig. 7** Steel02 stress–strain relations

3 Analytical Model of the Bridge

The considered bridge was designed and constructed as per AASHTO LRFD bridge design Specification (2007), AASHTO Guide Specifications for LRFD Seismic bridge design-2010 and Caltrans (2006) (Fig. 1). It consists of three spans with 105 m, 130 m, 100 m length separated by two 100-mm expansion joints (EXP) between the continuous spans. Figure 1a depicts the 30° curvature that pertains to the span leading to abutment 2 (AB2), while the 83° pertains to span 2 of the bridge. The bridge contains two horizontal curvatures with 30 degrees and 83 degrees subtended angles. The superstructure deck consists of three-cell cast in place concrete box girder with two interior webs. The intermediate joints are located at the top bent cap on the mid piers. The substructure consists of 11 single columns along the length of the box girder deck. Each column is a rectangular section with 1.30×1.10 m in dimensions except pier 6 which is located at the second curve with dimension of 1.50×1.30 m. Further typical details regarding the number of transverse and longitudinal reinforcing steel bars as well as their respective steel ratios are provided in Fig. 2. The longitudinal reinforcing steel ratio for 1.10×1.30 square meter columns is 2%. The abutments are seat typed with PTFE/Elastomeric bearings under the box girder deck as shown in Fig. 3. It should be noted that due to the presence of two mid expansion joints the longitudinal movement of the decks is limited, and modeling details of the expansion joints are discussed through the following sections. The bridge has shear keys at four different locations, two at each abutment (AB) and two at each bent cap in expansion joint.

The bridge is designed for high seismic zone with Design Base Acceleration (DBA) of 0.3 g. There are no restrainer cables designed for the superstructure movement reduction.

A 3-D finite element model of the bridge is developed in OpenSees environment. Figure 4 illustrates an overview of the model and its components. In this model, both material and geometrical nonlinearities are considered. Damping is modeled as Rayleigh viscous damping with the ratio of 0.05. Regarding the confined and unconfined concrete constitutive models, OpenSees facilitates the modeling procedure by presenting wide range of constitutive models and elements for various cross sections and materials. Fiber elements defined in this platform allow the researchers to allocate various parameters and characteristics to the material under study, making it easier to assign confined and unconfined behavioral characteristics to the element. Moreover, the fiber element allows for allocation of rebar location and sizes on the fiber sectional area. To model the behavioral characteristics of concrete pertaining to various bridge components, Concrete07 material shown in Fig. 5 is chosen. This model is the most recent one defined in the OpenSees platform, in order to define confined and unconfined concrete's stress–strain curve, Concrete07 is defined according to the model presented by Chang and Mander (1994). The concrete cover is defined by Concrete01 which is according to the model presented by Kent–Park–Scott (Scott 1982). To define the tensile parameters in the model, relationships presented by Mander et al. (1983, 1988) are used (Figure 6).

The portion of the cross section that constitutes the confined concrete bound by stirrups or FRP bonds is modeled by defining "Confined Concrete01" material. The relations

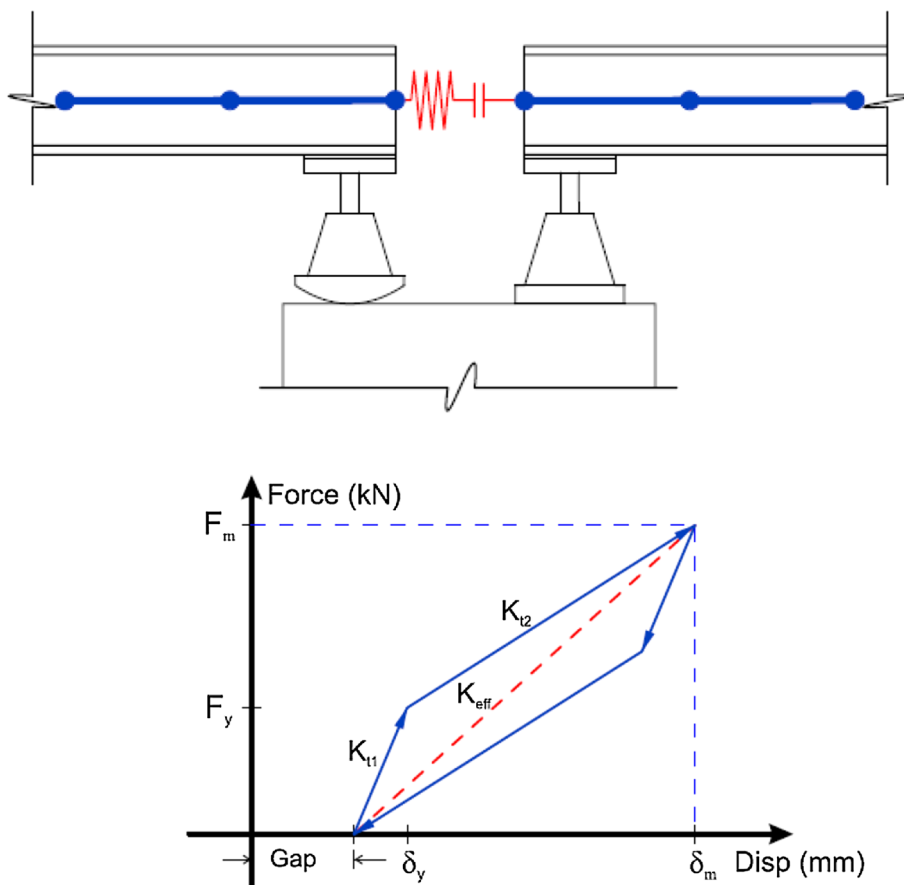**Fig. 9** Pounding action model in the software (Nielson 2007; Nielson and DesRoches 2007; Muthukumar 2003)

Table 1 Melloland bridge, result verification and comparison (Photo courtesy of Elnashai et al. 2002)

Researchers	First mode (s)	Second mode (s)
Zamiri et al. (2017)	0.42	0.33
Werner (1994)	0.39	–
Zhang and Makris (2001)	0.49	0.35
Elnashai et al. (2002)	0.32	0.31

Table 2 Capacity medians for bridge columns (Yi et al. 2007)

Description	Damage states	Drift ratio
Cracking and spalling	Slight	0.007
Loss of anchorage	Moderate	0.015
Incipient column collapse	Extensive	0.025
Column collapse	Complete	0.05

Fig. 10 Transverse fundamental mode obtained in the verification process, Melloland bridge (Zamiri et al. 2017)
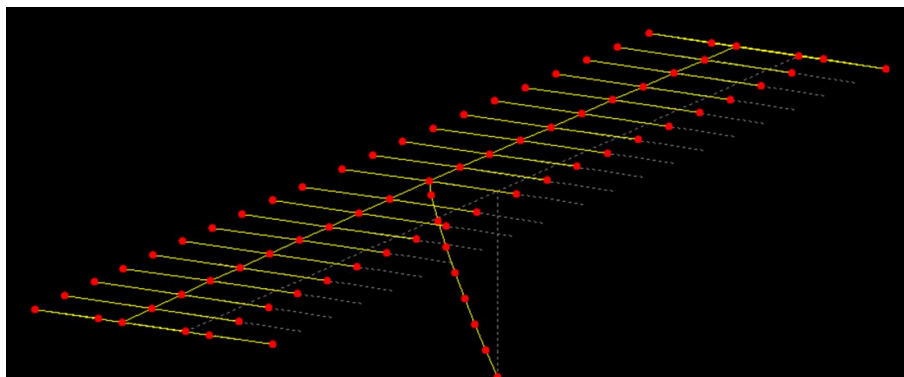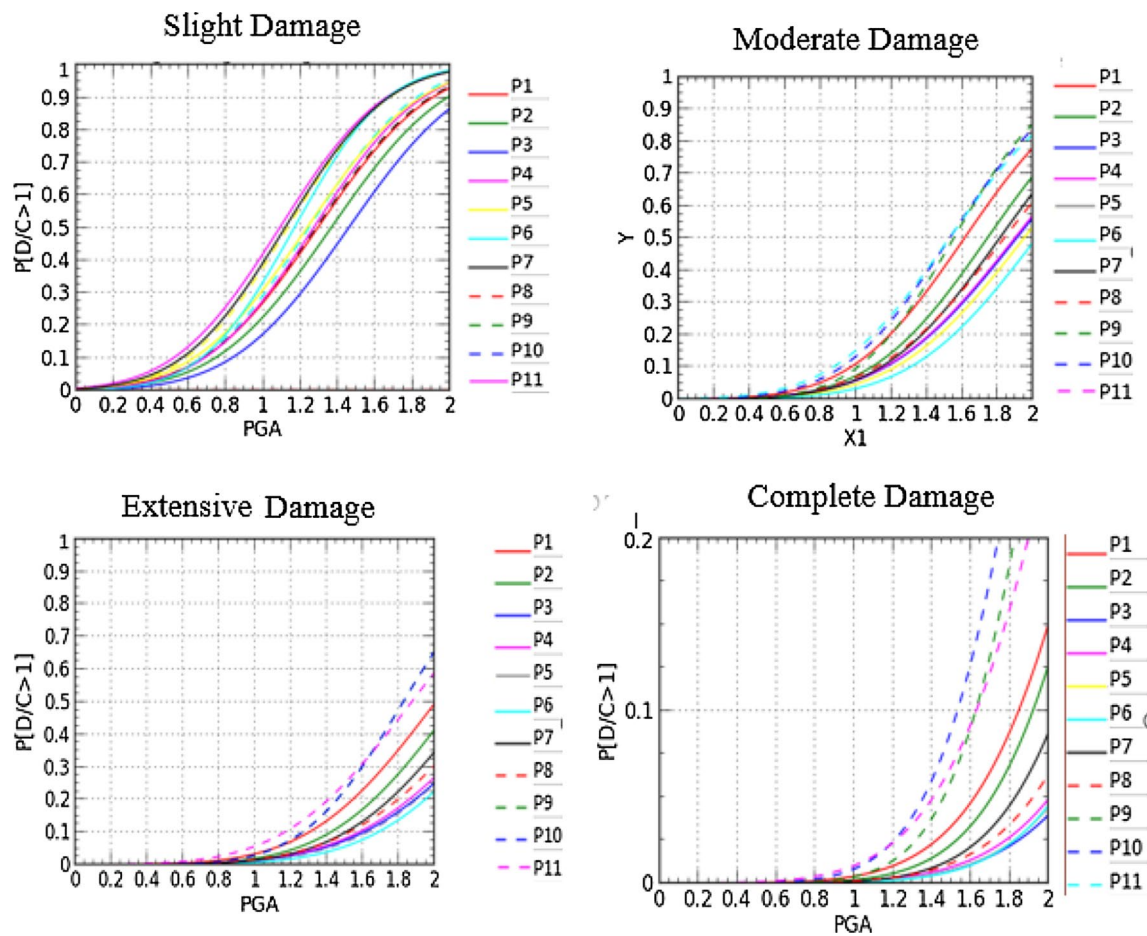
Fig. 11 Fragility curves of columns for four damage states

defined for this particular material in the OpenSees platform are defined following a study by Braga et al. (2006). In order to model the reinforcing steel bars, Steel02 material is used in the software platform given in Fig. 7. Steel02 stress–strain relations are based on the study by Giuffre–Manegotto–Pinto (Manegotto and Pinto 1973). This model is based on uniaxial strain hardening with the ability to accommodate "Bauschinger" effect, and the tangential stiffness during loading and unloading is essential with respect to this model.

The box girder deck is modeled by the grillage method and using Elastic Beam–Column elements. According to Caltrans (2006), modeling the deck of the bridges with straight geometry with one node pertaining to each beginning and end of the spans would not be accurate for horizontally curved bridges. This is due to the fact that the response of the bridge in each direction is coupled for this type of bridge. Therefore, the grillage model is employed to account for not only the box girder deck of the bridge but also the coupled responses. In the model, the mass of the deck was accurately distributed. To capture the nonlinear behavior of the piers, nonlinear beam–column elements

with fiber section are used by assigning different properties for concrete cover, confined concrete core and reinforcing steel bars. It is noted that the high torsional stiffness of the box girder decks combined with various subtended angles of the deck will eventually lead to higher forces in the piers, thereby causing nonlinear and inelastic behavior in the piers. Bearings are considered as sacrificial elements designed for service load conditions. The bearings assigned for this bridge class are PTFE/Elastomeric sliding bearing type positioned at the two abutments and two at the two mid-span expansion joints. Steel01 material is used for modeling of these bearings with zero-length element sections. Shear keys are located at the simply supported abutments and at the two mid-span expansion joints. For modeling these external shear keys, zero-length element section with hysteretic behavior material is considered (Chopra and Goel 2008). In reference to an experimental study conducted by Megally and Silva (2001), at University of San Diego on different shear keys the hysteretic behavior proposed by them was selected (Fig. 8). Following these studies, all the shear keys designed as per AASHTO specifications incurred a 90 mm

Fig. 12 Fragility curves for longitudinal displacements of PTFE bearing located at abutment #1
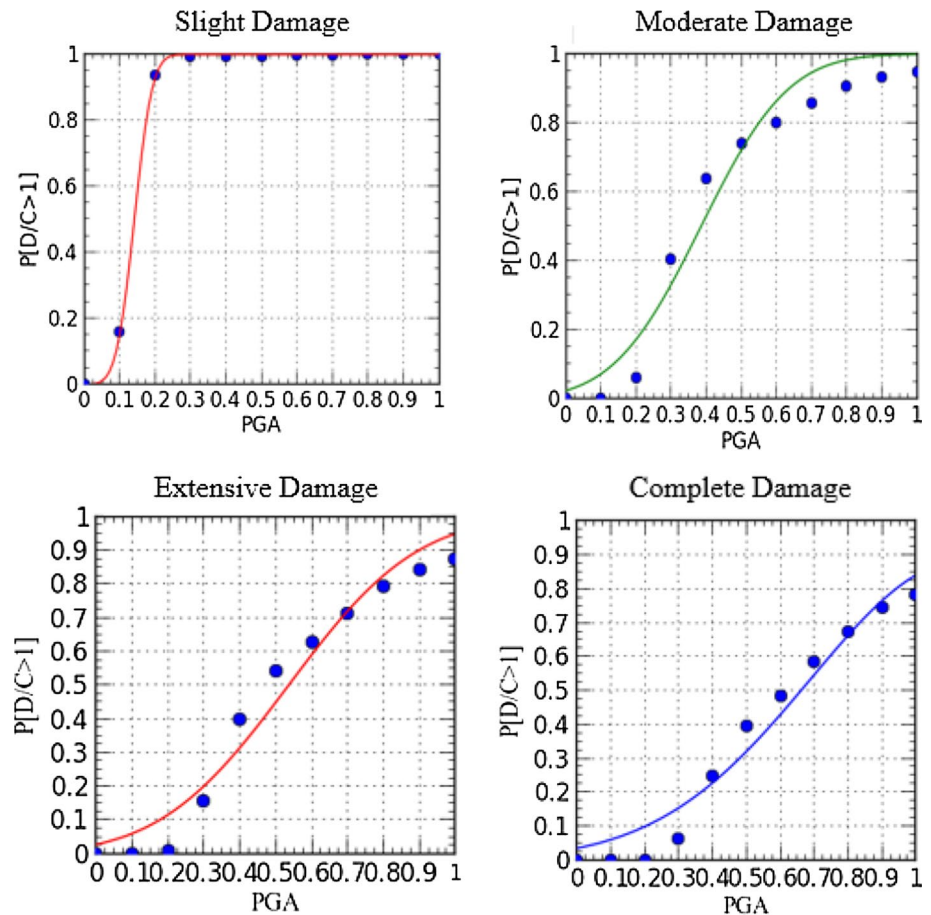
displacement prior to their failure. For modeling the probability of deck-to-deck and deck-to-abutment impact during seismic excitation of the bridge, the method recommended by Muthukumar (2003) was implemented. The material characteristics pertaining to the pounding action of the superstructure are accounted for by ElasticPPGap uniaxial material combined with a TwoNodeLink element in order to capture the dissipation of energy (Fig. 9). This model constitutes a bilinear behavior, in order to accommodate the pounding action. Following the study by Nielson (2007), two stiffness parameters K_{t1}, K_{t2}, yielding limit displacement δ_y and maximum displacement are defined. Owing to the presence of geogrid backwalls at the two abutments, modeling of the soil–structure interaction liquefaction of the backfill soil and active and passive soil pressure by the use of springs have been neglected.

3.1 Model Verification

Prior to the analysis procedure verification of the software code is essential. The analytical model used in this research conforms suitably with those given by Padgett (2007). The dynamic response complexity of curved bridges doubles the effort to verify the code. Therefore, the response

corresponding to a bridge with pre-existing data that have been previously recorded by onsite accelerometers versus those obtained by the software is compared; furthermore, the periods pertaining to each mode are given in Table 1. According to results obtained by real time data, the maximum bending moment at the footing of the piers is computed as 2485 Kn, whereas the maximum bending moment obtained by the code in this research is calculated as 2362 Kn, showing only 5% discrepancy, attesting to the analytical model used in this study. Results presented in Table 1 depict a 1% error as opposed to other researchers' works. These results also show that one can obtain close prediction of realities by considering less complex models. Figure 10 depicts the transverse mode pertaining to the Melloland bridge which conforms to other researchers' studies.

3.2 Ground Motion Suits

For nonlinear time history analysis of the bridge models, the acceleration time history spectrum is selected such that it conforms to the site conditions and characteristics. The ground motions are selected based on the fact that they satisfy the as-built bridge earthquake design in which the effects of magnitude, distance from the fault are considered.

Fig. 13 Fragility curves for transverse displacements of PTFE bearing located at abutment #1
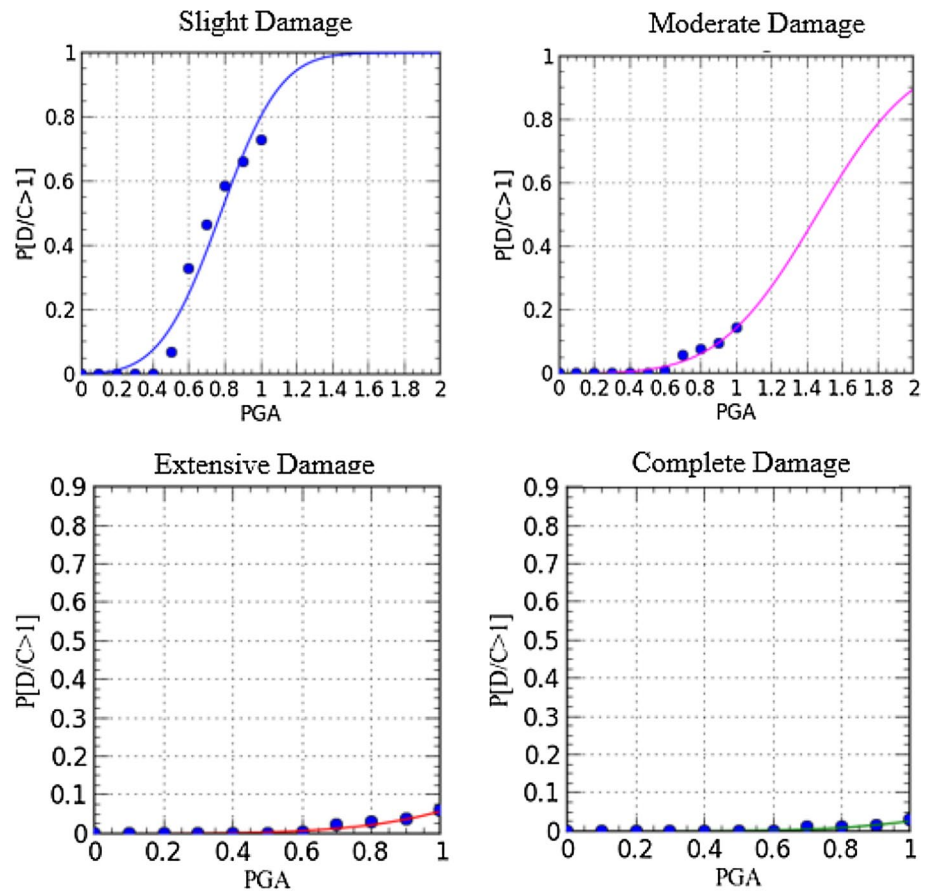

Therefore, a suit of 14 pairs of ground motions are selected and scaled relative to the design-based-acceleration (DBA) of bridges in this study which was 0.3 g. The soil at bridge site is categorized as type C based on the shop drawings. The response spectrum is scaled for a type C soil. To achieve a rather consistent outcome, the characteristics of the selected ground motion suits should be comparable, as they are in this study. All the selected ground motions were near-fault records (Table 3).

4 Fragility Analysis

Demand and capacity of a structure are two prime parameters in the fragility analysis process. A logarithmic normal distribution is considered for each of these decisive parameters, which will be presented by their means and their standard deviations. The median and the standard deviation of the demand are calculated utilizing regression analysis on a collection of computed bridge component responses. The median and the standard deviation of the capacity of the structure are calculated from the experimental results from existing studies on previous earthquake records Padgett (2007). Using Eqs. (3) and (4), required parameters for

fragility curves pertaining to each component under study will be calculated. In this study, the intensity measure considered is the peak ground acceleration (PGA). The PGA is applied to the structure in the range of 0.1–2 g. Subsequently, the components' responses are recorded and postprocessed resulting in fragility curves for each bridge component. The aforementioned process is repeated for each of the four assumed levels of damage. The structural components have been categorized in two groups of primary and secondary members in order to investigate the functional state of bridge such as traffic restrictions and repairing time. The fragility curves of the bridge structural system are calculated using probability seismic demand models (PSDMs) through a probabilistic approach. Slight, moderate, extensive and complete damage levels are the four damage limit states considered based on various risk assessment tools, namely HAZUS for the primary members such as piers and abutment supporting seat length. As far as the secondary members are concerned, since failure to these members may ultimately result in reduction of traffic speed, considering only the first two damage states will suffice. The capacity limit states are defined such that they are in accord with corresponding system limit states.

Fig. 14 Fragility curves for longitudinal displacements of PTFE bearing located at abutment #2
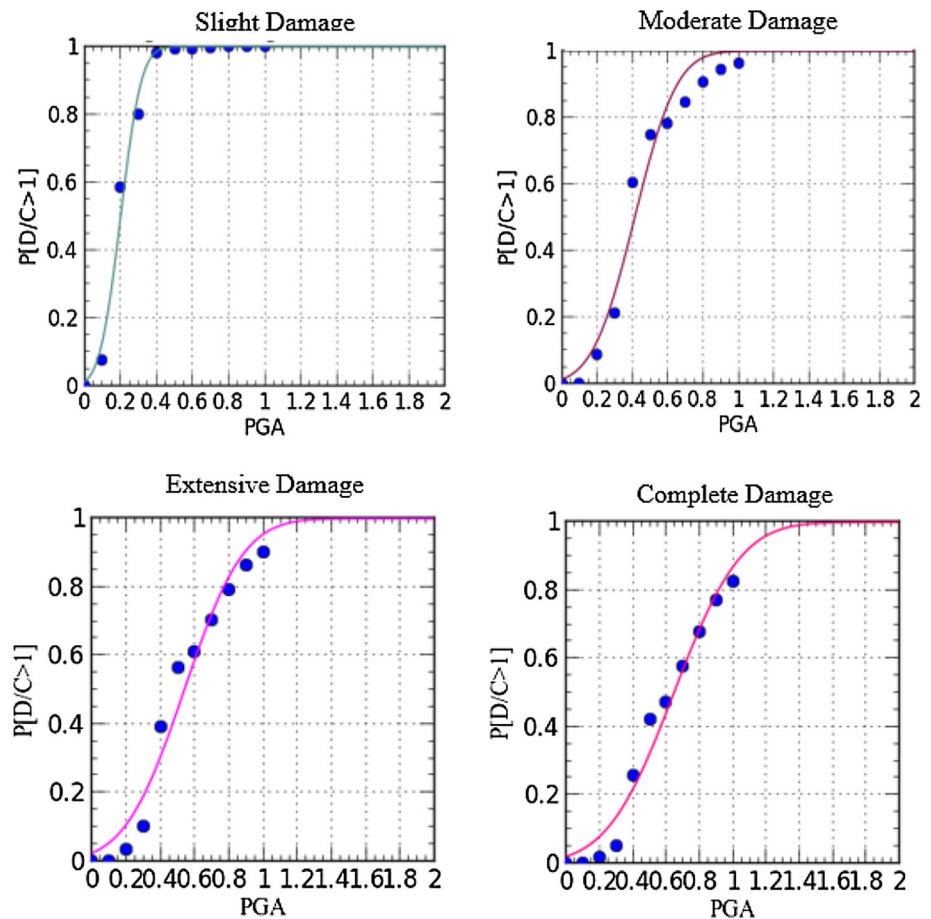
A particular limit state for one component should have an analogous impact on the performance of the entire bridge system the same as other components do Padgett et al. (2008). The limit states as well as the corresponding medians and standard deviations considering the pier drift ratio damage states are adapted based on the study conducted by Yi et al. and are presented in Table 2.

According to a study by Konstantinidis et al. (2008), when the deformation of PTFE\Elastomeric bearing reaches 75 mm, it requires inspection due to minor wear subsequently leading to slight damage state. By reaching a deformation of 125 mm, the PTFE bearing will require imminent repair and resurfacing according to experimental studies resulting in level two limit state of moderate damage state for this so-called secondary member. As far as the shear keys of the bridge model are concerned following the study implemented by Megally and Silva (2001), at the university of San Diego California, slight and moderate damage states are considered with 40 mm and 100 mm displacements accordingly. It is worth mentioning that in the slight damage limit state minor cracks will appear in the shear keys.

For the moderate damage limit state, new shear keys will replace the damaged ones.

By regression analysis of the maximum responses recorded for each component, the *a* and *b* parameters presented in Eq. 1a and 1b are calculated. Eventually, by augmenting the capacity and demand limit states in Eq. 4 the fragility curves pertaining to bridge components are calculated and drawn.

5 Results

The detailed 3D finite element model of the considered bridge is modeled using OpenSees platform. Probabilistic approach has been implemented in order to evaluate seismic response and behavior of the bridge under normal and critical conditions. Seven pairs of ground motions have been applied to the model; eventually, fragility curves of the components are calculated. Due to the asymmetrical geometry of the bridge in plan, i.e., the double curvature deck, the bridge contains three span lengths, 335 m in total and is doubly curved in plan. The pier fragility curves demonstrate

Fig. 15 Fragility curves for transverse displacements of PTFE bearing located at abutment #2
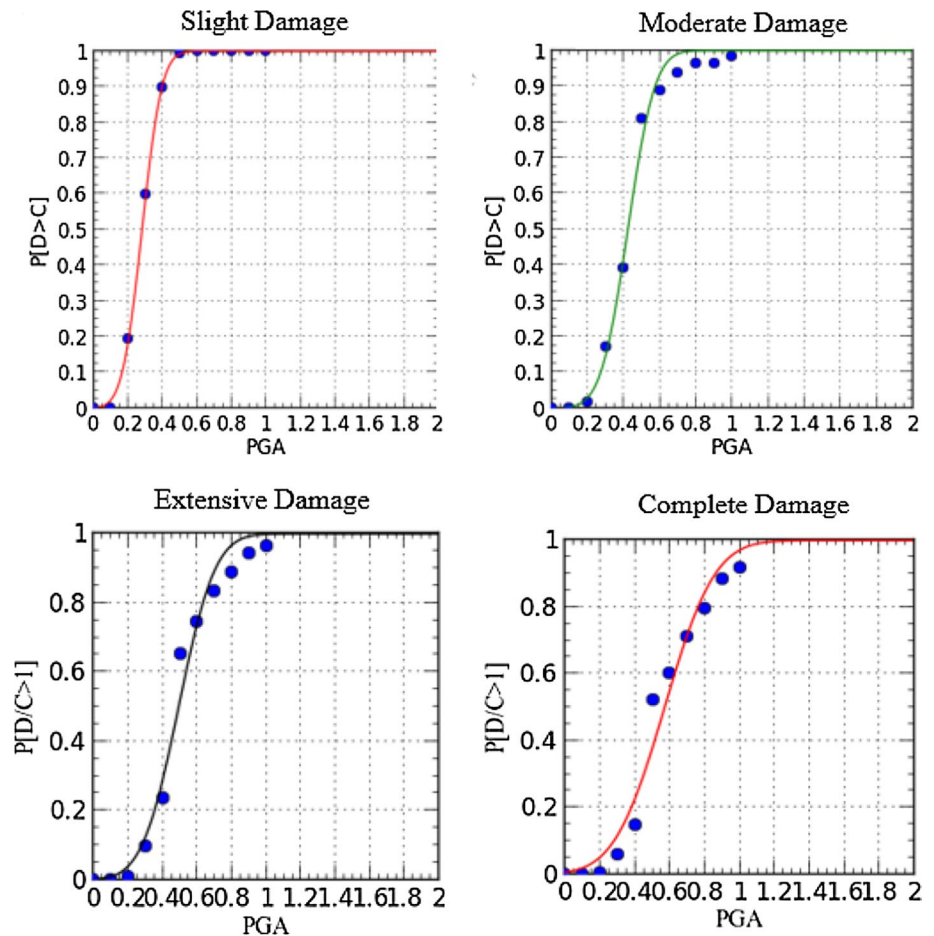

an appropriate response. Among the 11 piers of the bridge, pier number 11 which is located next to abutment number two is more susceptible to damage for all four damage states. Figure 11 depicts pier fragility and probability of failure pertaining to each damage state; the results are extrapolated for PGAs up to 2 g. Based on the column fragility curves and the geometry of the bridge, the following results are concluded. Primarily, columns P5, P6 and P7 that shape the horizontal curvature of the deck with larger subtended angle become more fragile in the slight damage state as opposed to other columns. The column, #P11, located immediately before abutment 2 (AB2) is the most fragile one. For moderate, extensive and complete damage states columns P11 and P10 are more fragile than the rest. The overall column fragilities implicate proper behavior with highest probability of failure of 0.4 relating to P11 for PGA (DBA) 0.3 g. Abutment #1 which is located at the end of span 3 depicts higher probability of failure with respect to longitudinal

displacements for all the four fragility damage states. i.e., 95, 40, 18 and 8% probability of failure for slight, moderate, extensive and complete damage states (Fig. 12). This can be prevented by retrofit measures such as restrainer cables. On the other hand, the transverse response of PTFE bearings shows appropriate behavior under 0.3 g DBA with respect to all four fragility states (Fig. 13).

80, 20, 15 and 5% probability of failure for slight, moderate, extensive and complete damage states have been obtained for the longitudinal response of AB2 with respect to the 0.3 g DBA. However, the transverse response of abutment 2 attests to the fact that response of the structure in span 2 with larger subtended angle affects the span 1, which then affects the PTFE bearing response located in abutment 2. The probabilities of failure for 0.3 g PGA with respect to slight, moderate, extensive and complete damage states are 60, 40, 10 and 5%. It can be concluded that the difference between AB1 and AB2 transverse response is due to

Fig. 16 Fragility curves for longitudinal displacements of PTFE bearing located at mid-span of the end of span #3 for all damage states
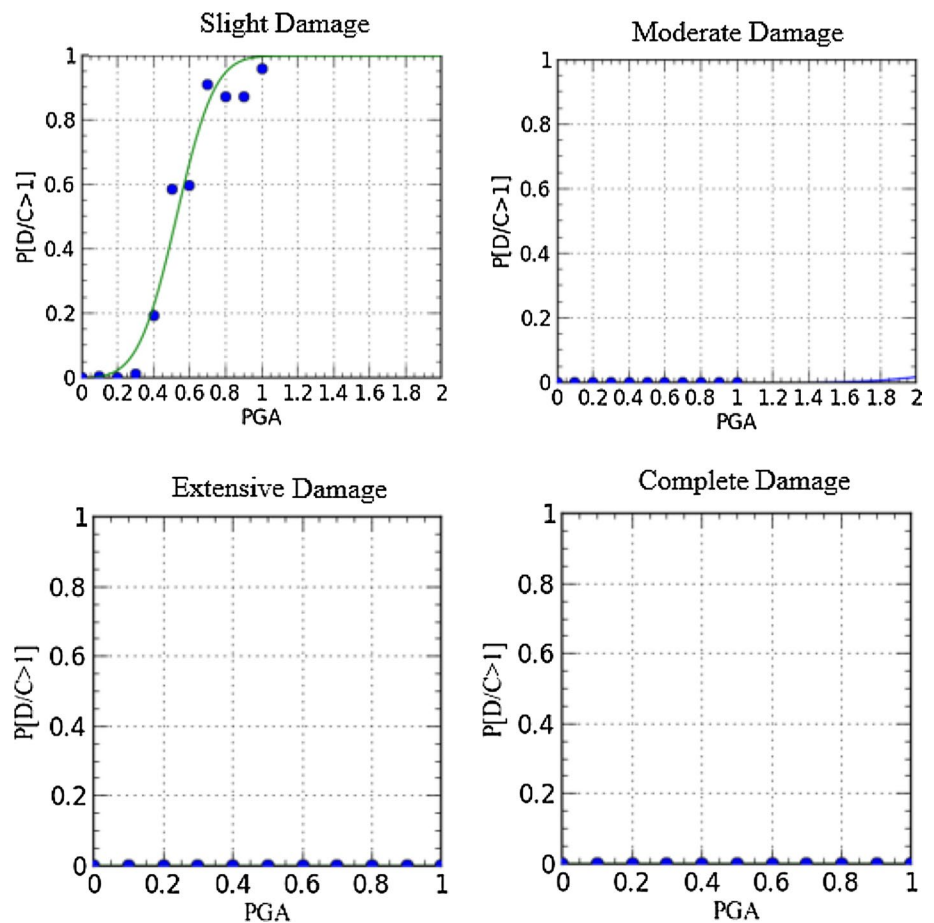

the coupled effect and larger subtended angle of span 2 as opposed to span 3. PTFE responses of the two expansion joints show the same results as the two abutments; in other words, the longitudinal response of EXP1 slight damage state shows less than 5% probability of failure with respect to 0.3 g DBA versus 35% for EXP2 longitudinal response which is located just after the larger subtended angle of span 2. Furthermore, the transverse response under the 0.3 g PGA of EXP1 depicts less than 5% probability of failure pertaining to the slight damage as opposed to the nearly 15% probability failure of EXP 2 for the same damage state (Figs. 14, 15, 16, 17, 18, 19).

Four locations of shear keys were determined for this model, and the results of their fragility analyses are presented in Figs. 20, 21, 22 and 23. Probabilities of failure have been calculated for slight and moderate damage states only, which follows the same procedure in the literature. The shear key positioned at the location of abutment 1 (SK1) shows less than 5% for both of the slight and moderate

damage states at PGA of 0.3 g. Diversely the shear key pertaining to abutment 2 (SK2) has shown 40 and 30% probability of failure with respect to slight and moderate damage states, respectively, for the same PGA (0.3 g). The shear keys located at expansion joint 1 have depicted less than 5% probability of failure at PGA 0.3 g with regard to slight and moderate damage states, respectively. However, the shear keys located at expansion joint 2 which is at the end of span 2 possessing the larger subtended angle show 19% and 10% probability failure with respect to slight and moderate damage states for PGA 0.3 g. These results also conform to the effect of the coupled responses in orthogonal directions for the larger subtended angles. By interpreting the results of the fragility analysis of abutment 1 nodes, it can be deduced that longitudinal response of the bridge deck under 0.3 g PGA will cause impaction between deck and abutment wall and result in 40% failure in slight damage state. Same results are obtained with regard to the nodes of expansion joint 1 with 40% probability of failure with respect to slight damage

Fig. 17 Fragility curves for transverse displacements of PTFE bearing located at mid-span of the end of span #3 for all damage states
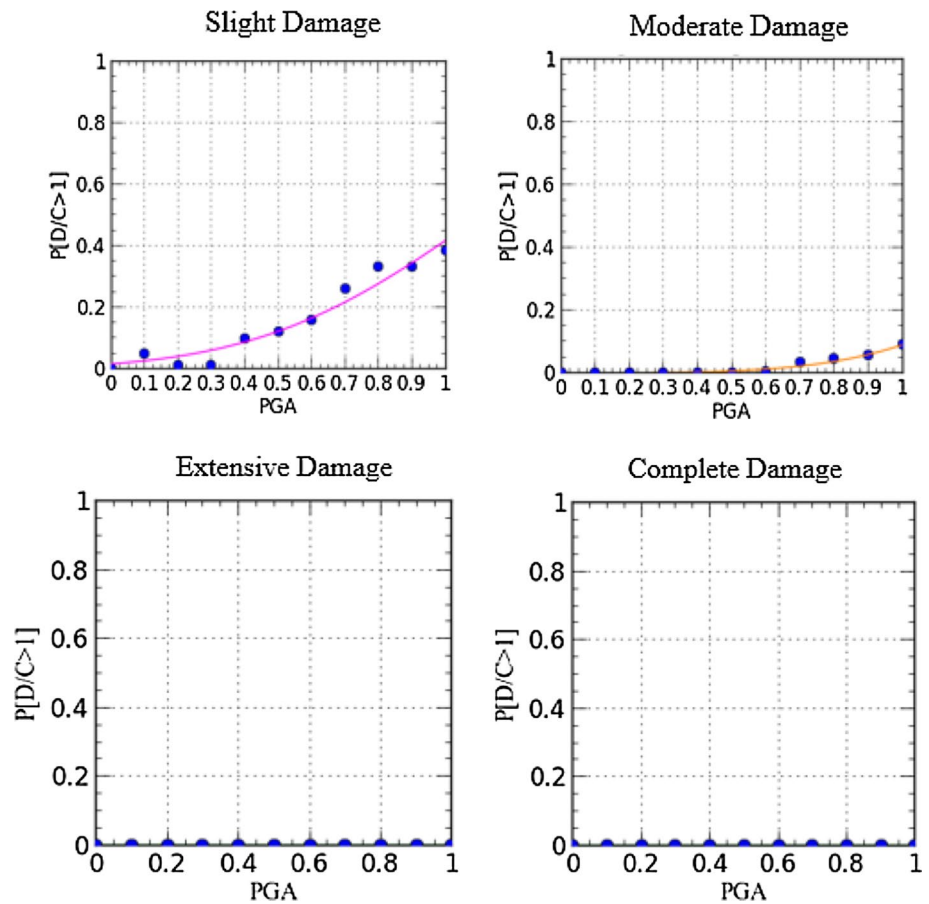
state. However, results of EXP2 show larger deck–deck impact, with 45% probability of failure in slight damage state in EXP2 as opposed to 25% probability of failure for deck-abutment impact with respect to the node of abutment 2 (Figs. 24, 25, 26).

Lastly, component fragility curves of this model have been superimposed and are presented in Fig. 27.

6 Conclusions

This study attempts to evaluate the seismic vulnerability of a specific class of horizontally double curved reinforced concrete box girder bridges in the as-built condition. Fragility curves of the components have been calculated. Due to the asymmetrical geometry of the bridge in plan, i.e., the double curvature deck, seismic responses in orthogonal directions (tangential and radial) are coupled. It results in higher demand during seismic excitations. The coupling

effect becomes more distinguished with respect to span 2; this is due to the larger subtended angle of this span versus span 3, which will eventually lead the structural system or components to states that are more vulnerable.

The effect of the earthquake frequency content in near-fault versus far-fault earthquakes could be a decisive factor in the elastic and inelastic response analysis. Near-fault ground motions contain pulses with longer periods; therefore, the impact on the structure is larger than far-field accelerations. Due to the presence of the faults with various potential activities near the bridge, appropriate measures regarding the reduction of the components' displacements should be taken into account. Furthermore, the location of the bridge on soil type C will cause the seismic excitation to intensify and incur more damage to the entire structure. The subtended angle appears to have adverse effects on support displacements as well as deformations at PTFE bearings. The two abutments incur most of the damage. The excess longitudinal movement of the two bearings could

Fig. 18 Fragility curves for longitudinal displacements of PTFE bearing located at mid-span of the end of span #2 for all damage states
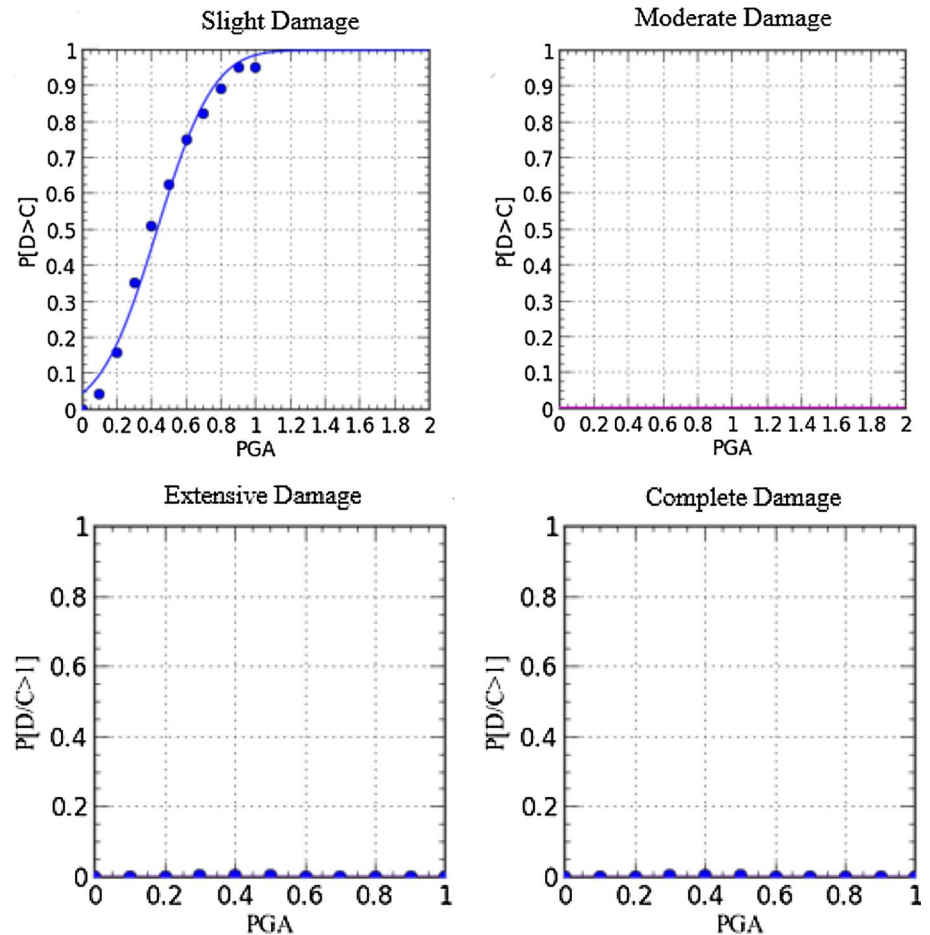
induce pounding to the geogrid backwalls located at the two abutments.

Finally, there are certain measures that a designer should take into account in order to reduce the adverse effects of the curvature angles, i.e., subtended angles of the bridge deck on the seismic response of the components as well as the structural bridge system. The alleviation of the damage to the bridge could be refrained at the design phase by increasing the deformation capacity of the components if economically feasible. On the other hand, depending on the damage type certain retrofit scenarios could be proposed.

The nonlinear time history analysis indicated that for CHICHI-Taiwan earthquake which is a near-fault earthquake with magnitude 7.0 the component responses increased by a factor of 4–5. This could be due to the fact that the frequency content of the ground motion is near that of the structure. Another conjecture for this immense increase in responses could be the effect of coupled longitudinal and transverse responses regarding bridge components. In recent studies on seismic fragility assessment of bridges with horizontal curvature it was deduced that columns are the most vulnerable components. Nonetheless, in this study the column fragility curves indicated proper responses. Among 11 piers of the bridge, fragility curve of Pier #11 demonstrated the most vulnerability with 41% probability of failure at PGA of 1 g, and nearly 2% failure pertaining to PGA of 1 g in the complete damage state. The moment–curvature analysis of bridge column details has implicated an ultimate curvature capacity of 0.1217 1/m and curvature at first yield of 3.156E−3 1/m. The ultimate moment capacity of pier #2 is 7900 kN m. It should be noted that the moment demands about the longitudinal and the tangential axes for this column have been shown to be 8600 kN m and 5100 kN m pertaining to PGA of 1.0 g.

Fig. 19 Fragility curves for transverse displacements of PTFE bearing located at mid-span of the end of span #2 for all damage states
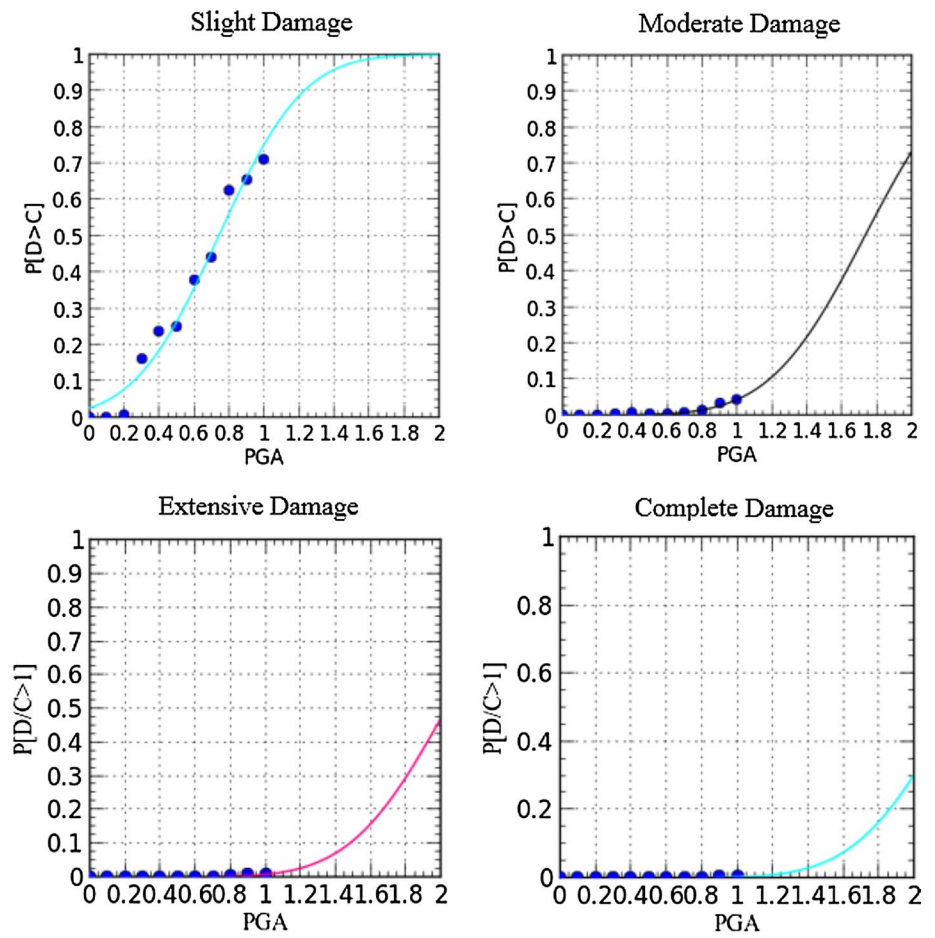

Fig. 20 Abutment 1 shear key fragility curves pertaining to slight and moderate damage states
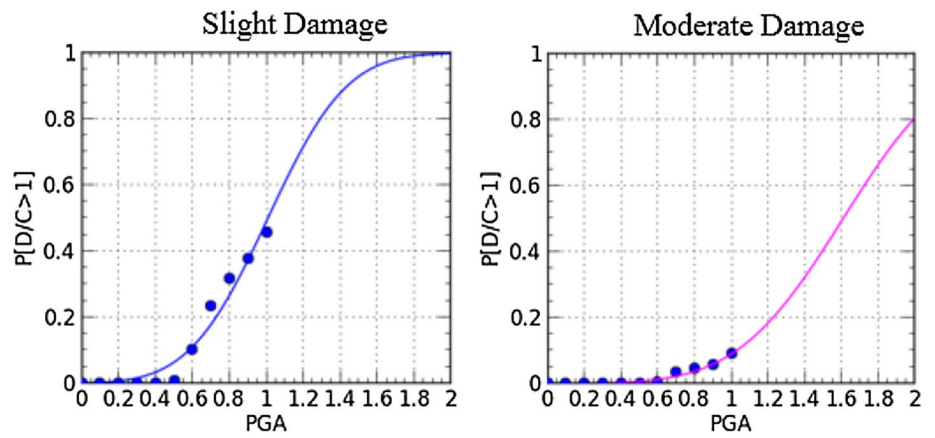
Fig. 21 Abutment 2 shear key fragility curves pertaining to slight and moderate damage states
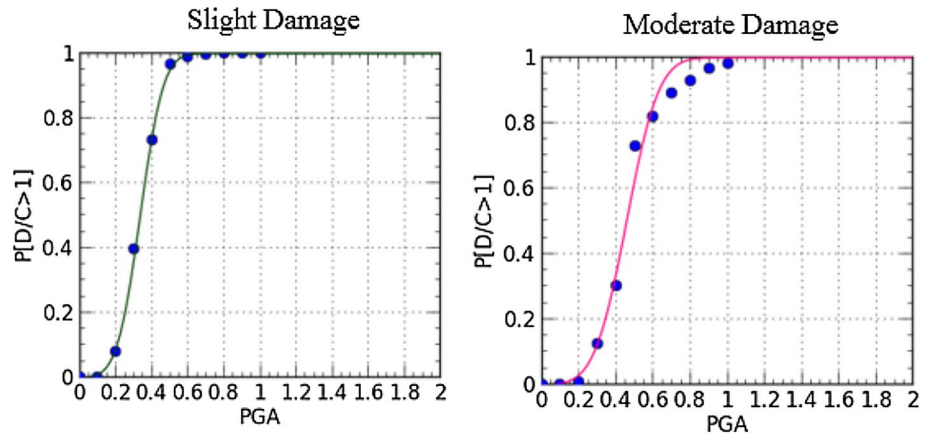

Fig. 22 Shear key fragility curves pertaining to slight and moderate damage states for span 3 and span 2 connection at expansion joint 1
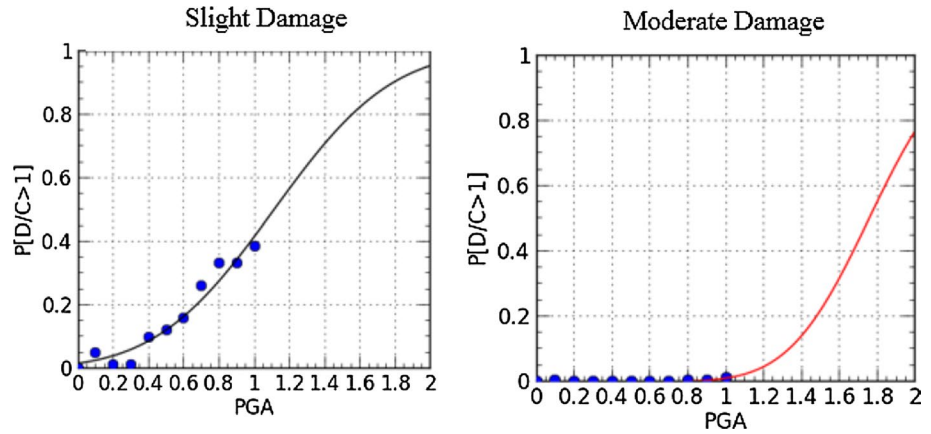

Fig. 23 Shear key fragility curves pertaining to slight and moderate damage states for span 2 and span 1 connection at expansion joint 2
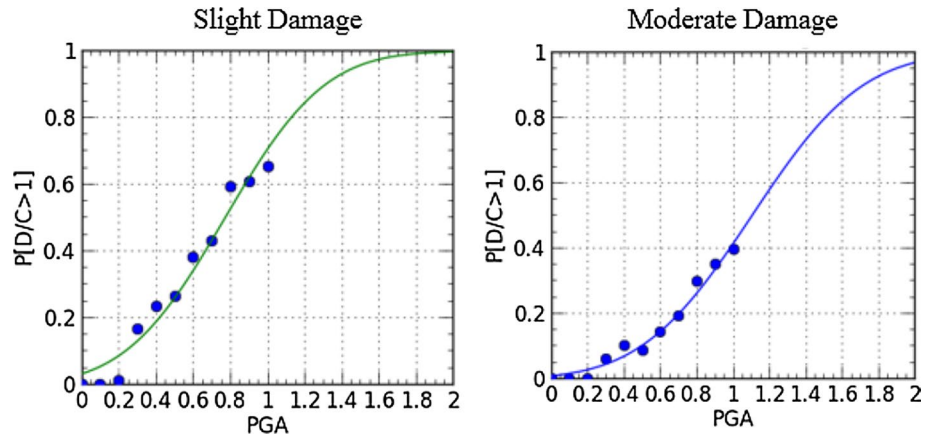
Fig. 24 Deck-abutment impact fragility curves of abutment 1 in slight and moderate damage states
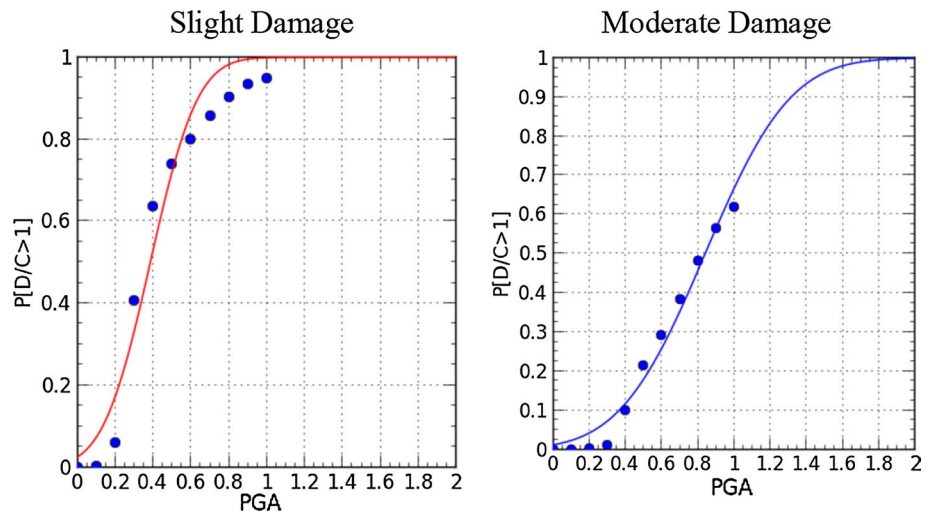

Fig. 25 Deck–deck impact fragility curves of (**a**) EXP1, (**b**) EXP2 in slight and moderate damage states
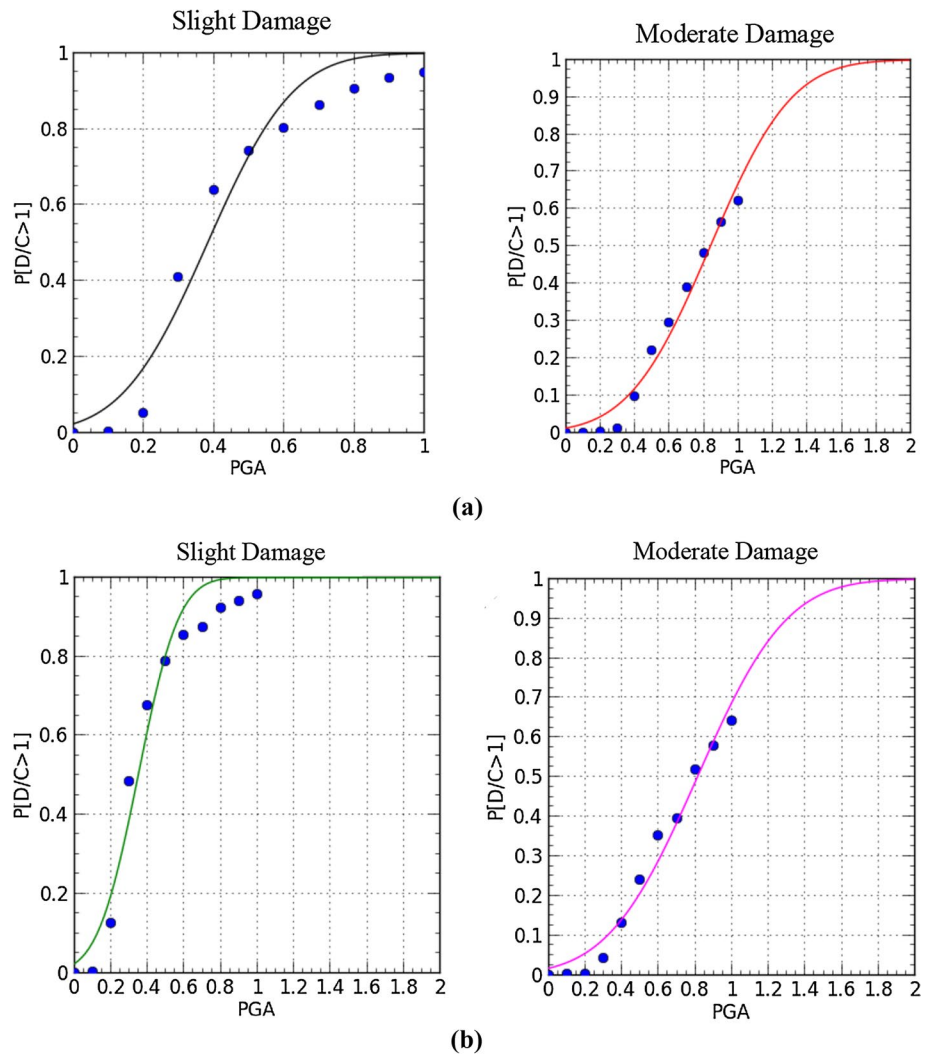

(a)

(b)

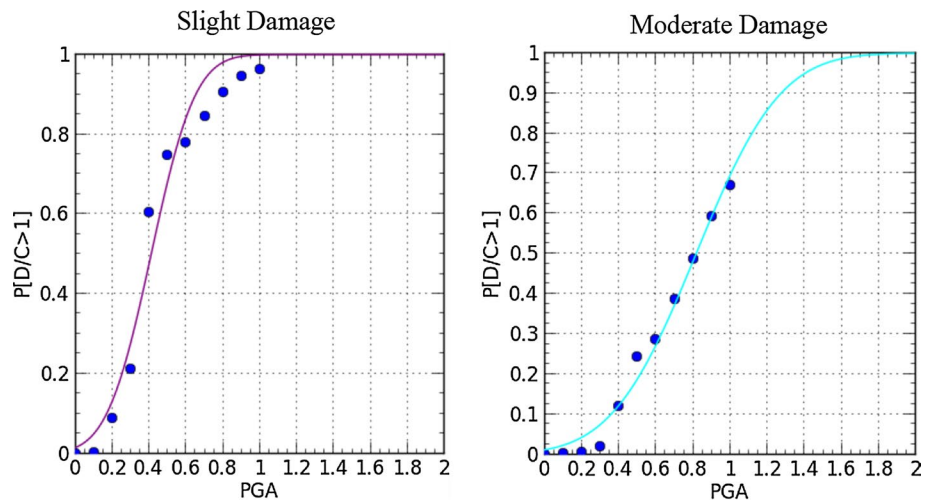**Fig. 26** Deck–deck impact fragility curves of abutment 2 in slight and moderate damage states

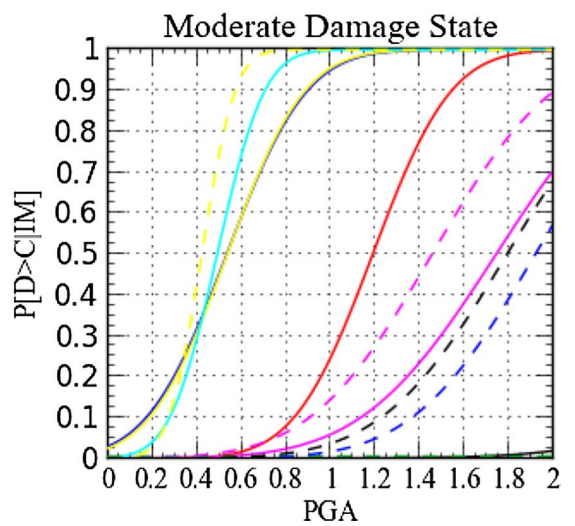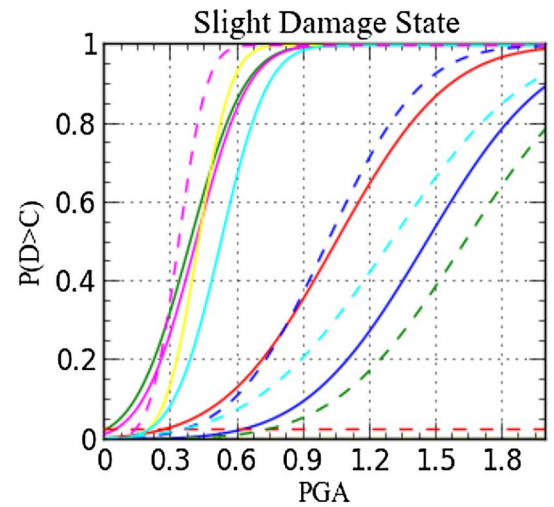**Fig. 27** Component fragility curves, slight and moderate damage levels

Table 3 Selected ground motion suites applied to the model in this study

W	Earthquake	Date	Station location	Magnitude (M)	Component	Distance (km)	PGA (g)	Scaled PGA (g)	PGV (mm/s)	PGD (mm)
1	Chi-Chi, Taiwan	09/20/1999	CHY101	7.6	W	11.14	0.353	0.596	706	452.8
2	Chi-Chi, Taiwan	09/20/1999	CHY101	7.6	N	11.14	0.440	0.596	1150	687.5
3	Imperial Valley	10/15/1979	5058 El Centro Array #11	6.9	230	12.6	0.380	1.154	421	185.9
4	Imperial Valley	10/15/197	5058 El Centro Array #11	6.9	140	12.6	0.364	1.154	345	160.7
5	Loma Prieta	10/18/1989	47380 Gilroy Array #3	7.1	0	14.4	0.555	0.813	357	82.1
6	Loma Prieta	10/18/1989	47380 Gilroy Array #3	7.1	90	14.4	0.367	0.813	447	192.5
7	Northridge	01/17/1994	90053 Canoga Park-Topanga Can	6.7	106	15.8	0.356	0.562	321	91.3
8	Northridge	01/17/1994	90053 Canoga Park-Topanga Can	6.7	196	15.8	0.420	0.562	608	201.7
9	Superstition	11/24/1987	01335 El Centro Imp.Co. Cent	6.6	0	13.9	0.358	0.75	464	175.0
10	Superstition	11/24/1987	01335 El Centro Imp.Co. Cent	6.6	90	13.9	0.258	0.75	409	202.0
11	Northridge	01/17/1994	90057 Canyon Country-W Lost C.	6.7	0	13.0	0.410	0.664	430	117.5
12	Northridge	01/17/1994	90057 Canyon Country-W Lost C.	6.7	270	13.0	0.482	0.664	451	125.8
13	Loma Prieta	10/18/1989	47380 Gilroy Array #2	7.1	0	12.7	0.367	0.705	329	71.5
14	Loma Prieta	10/18/1989	47380 Gilroy Array #2	7.1	90	12.7	0.322	0.705	391	120.7

To achieve a rather consistent outcome, the characteristics of the selected ground motion suits should be comparable, as they are in this study. All the selected ground motions were near-fault records (Table 3). Geometrical irregularities of a road and presence of active and semi-active faults in the proximity of the bridge construction site require this type of analysis for obtaining a more accurate and realistic approach.

References

AASHTO (2007) LRFD bridge design specifications. American Association of State Highway and Transportation Officials, Washington, DC

Braga F, Gigliotti R, Laterza M, D'Amato M, Kunnath S (2006) Modified steel bar model incorporating bond-slip for seismic assessment of concrete structures. J Struct Eng 138(11):1342–1350

Caltrans (2006) Caltrans seismic design criteria, 1st edn. California Department of Transportation, Sacramento, CA

Chang GA, Mander JB (1994) Seismic energy based fatigue damage ananlysis of bridge columns: part 1 – evaluation of seismic capacity. NCEER technical report no. NCEER-94-0006, State University of New York, Buffalo, NY

Chopra AK, Goel K (2008) Role of shear keys in seismic behavior of bridges crossing fault-rupture zones. J Bridge Eng 13(4):398–408

Cornell AC, Jalayer F, Hamburger RO (2002) Probabilistic basis for 2000 SAC Federal Emergency Management Agency Steel Moment Frame Guidelines. J Struct Eng 128(4):526–532

Elnashai AS, Papanikolaou V, Lee D (2002) A system for inelastic analysis of structures. Mid-America Earthquake Center, University of Illinois at Urbana-Champaign

FEMA-350 (2000) Recommended seismic design criteria for new steel moment-frame buildings. SAC Joint Venture for the Federal Emergency Management Agency, Washington, DC

Itani AM, Reno ML (2000) Horizontally curved bridges. In: Chen W, Duan L (eds) Bridge engineering handbook

Kaviani P, Zareian F, Taciroglu E (2012) Seismic behavior of reinforced concrete bridges with skew-angled seat-type abutments. Eng Struct 45:137–150

Kim S-H, Shinozuka M (2003) Fragility curves for concrete bridges retrofitted by column jacketing and restrainers. In: Proceedings of the 6th US conference and workshop on lifeline earthquake engineering, pp 906–915

Konstantinidis D, Kelly J, Makris N (2008) Experimental investigation on the seismic response of bridge bearings. Earthquake Engineering Research Center, University of California

Mander J, Priestly M, Park R (1983) Seismic design of bridge piers. Research Report 84-02, University of Canterbury, Christchurch

Mander JB, Priestley MJN, Park R (1988) Observed stress–strain behavior of confined concrete. J Struct Eng 114(8):1827–1849

Mander JB, Kim DK, Chen SS, Premus GJ (1996) Response of steel bridge bearings to the reversed cyclic loading. Report No. NCEER 96-0014, NCEER

Manegotto M, Pinto PE (1973) Methods of analysis for cyclically loaded reinforced concrete plane frames. In: Proceedings of the IABSE symposium in resistance of ultimate deformability of structures acted on by well-defined repeated loads, Lisbon, pp 15–22

Megally SH, Silva PF (2001) Seismic response of sacrificial shear keys in bridge abutments. Department of Structural Engineering, University of California, San Diego

Monzon EV, Buckle IG, Itani AI (2013) Seismic performance of curved steel plate girder bridges with seismic isolation. Report 13-06, Center for Civil Engineering Earthquake Research, Department

of Civil and Environmental Engineering, University of Nevada, Reno, NV

Muthukumar S (2003) A contact element approach with hysteresis damping for the analysis and design of pounding in bridges. PhD thesis, Georgia Institute of Technology

Nielson BG (2007) Analytical fragility curves for highway bridges in moderate seismic zones. PhD dissertation, Georgia Institute of Technology

Nielson BG, DesRoches R (2007) Analytical seismic fragility curves for typical bridges in the central and southeastern United States. J Earthq Spect 23:615–633

Nutt, Redfield, Valentine (2008) Development of design specifications and commentary for horizontally curved concrete box-girder bridges. Report 620, National Cooperative Highway Research Program, Transportation Research Board, Washington, DC

OpenSees v. 2.4.4., (2005). "Open Source for Earthquake Engineering Simulation". Copyrighted at University Of California at Berkeley, United States

Padgett J (2007) Seismic vulnerability assessment of retrofitted bridges using probabilistic methods. PhD dissertation. Georgia-Tech University, United States

Padgett J, Nielson BG, DesRoches R (2008) Selection of optimal intensity measure for use in probabilistic seismic demand models of highway bridge portfolios. Earthq Eng Struct Dyn 37:711–725

Ramanathan NK (2012) Next generation seismic fragility curves for California bridges incorporating the evolution in seismic design philosophy. PhD thesis, Georgia Institute of Technology, Atlanta

Ramanathan K, DesRoches R, Padgett JE (2010) Analytical fragility curves for multispan continuous steel girder bridges in moderate seismic zones. Transp Res Rec 2202:173–182

Scott B, Park R, Priestly M (1982) Stress–strain behavior of concrete confined by overlapping hoops at low and high strain rates. J Am Concr Inst 79:13–27

Shinozuka M, Kim S-H, Yi J-H, Kushiyama S (2002) Fragility curves of concrete bridges retrofitted by column jacketing. J Earthq Eng Eng Vib 01(2):195–205

Tondini N, Stojadinović B (2012) Probabilistic sesimic demand model for curved reinforced concrete bridges. Bull Earthq Eng 10:1455–1479

Werner SD (1994) Study of Caltrans' seismic evaluation procedure for short bridges. In: Proceeding 3rd annual seismic research workshop. California Department of Transportation, Sacramento

Yi JH, Kim SH, Kushiyama S (2007) PDF interpolation technique for seismic fragility analysis of bridges. Eng Struct 29(7):1312–1322

Zamiri A, Banan MR, Banan MR (2017) Fragility curves for horizontally curved reinforced concrete box girder bridges in as-built condition. Master of science thesis, Department of Civil and Environmental Engineering, Shiraz University, Shiraz

Zhang J, Makris N (2001) Seismic response analysis of highway over-crossings including soil–structure interaction. PEER report no. 2001/02